crystals

MDPI

Article

Influence of Amino Acids on Calcium Oxalate Precipitation in Systems of Different Chemical Complexity

Anamarija Stanković [1,*], Nives Matijaković Mlinarić [2], Jasminka Kontrec [2], Branka Njegić Džakula [2], Daniel M. Lyons [3], Berislav Marković [4] and Damir Kralj [2]

[1] Department of Chemistry, University of Osijek, Ulica cara Hadrijana 8/A, 31000 Osijek, Croatia
[2] Division of Materials Chemistry, Ruđer Bošković Institute, Bijenička cesta 54, 10000 Zagreb, Croatia; nives.matijakovic@irb.hr (N.M.M.); jasminka.kontrec@irb.hr (J.K.); bnjeg@irb.hr (B.Nj.Dž.); kralj@irb.hr (D.K.)
[3] Center for Marine Research, Ruđer Bošković Institute, Giordano Paliaga 5, 52210 Rovinj, Croatia; lyons@irb.hr
[4] Faculty of Dental Medicine and Health Osijek, Crkvena 21, 31000 Osijek, Croatia; bmarkovic@fdmz.hr
* Correspondence: astankovic@kemija.unios.hr or ster.anamarija@gmail.com

Abstract: The mechanisms and conditions under which urinary stones, pathological biominerals in the kidneys and bladder, are formed have not yet been fully clarified. This study aims to understand the role of the system complexity and seven different amino acids (alanine, phenylalanine, glycine, serine, cysteine, histidine, and aspartic acid) in the spontaneous precipitation of calcium oxalate. To elucidate these effects, the conditions simulating hyperoxaluria ($c_i(Ca^{2+})$ = 7.5 mmol dm^{-3} and $c_i(C_2O_4^{2-})$ = 6.0 mmol dm^{-3}) were used for the first time. In this work, systematic research on calcium oxalate precipitation was performed in three systems of different chemical complexities: (a) only calcium and oxalate ions, (b) increased ionic strength, and (c) artificial urine at two initial pHs (pH_i = 5.0 and 9.0). In all the investigated systems, the dominant precipitation of calcium oxalate monohydrate (COM) was observed, except in the artificial urine system at pH_i = 9.0, in which a mixture of COM and calcium oxalate dihydrate (COD) was obtained. In all the investigated systems, a significant influence of the selected amino acids on the morphology and crystal growth of COM was observed, with more pronounced changes at pH_i = 9.0. Overall, polar amino acids and nonpolar phenylalanine inhibit the growth of COM, which is a more pathogenic hydrate form. The artificial urine system proved to be more relevant for the observation of effects relevant to kidney stone formation in the human body.

Keywords: calcium oxalate; pathological mineralization; hyperoxaluria; amino acids

Citation: Stanković, A.; Matijaković Mlinarić, N.; Kontrec, J.; Njegić Džakula, B.; Lyons, D.M.; Marković, B.; Kralj, D. Influence of Amino Acids on Calcium Oxalate Precipitation in Systems of Different Chemical Complexity. *Crystals* **2024**, *14*, 599. https://doi.org/10.3390/cryst14070599

Academic Editor: Ruikang Tang

Received: 6 June 2024
Revised: 21 June 2024
Accepted: 23 June 2024
Published: 28 June 2024

1. Introduction

Biomineralization is the process of producing functional organic–inorganic hybrid materials (biominerals) in living organisms. The biomineralization process involves the selective displacement of inorganic and organic chemical species (ions, molecules) from the respective tissues and their incorporation into functional superstructures, all of which are under strict biological control. The functions of biomineralized organs and tissues are very diverse (structural support, protection, navigability, food consumption, etc.). Contrary to biomineralization as a process in which new and functional materials are produced, pathological biomineralization is a process in which unwanted biomineralization occurs, in the form of deposits such as kidney or bladder stones, gallstones, caries, arterial plaques, etc. [1,2]. The specific form of pathological biomineralization is urolithiasis, a chronic, recurrent urinary tract disease resulting in urinary stones in different parts of the kidney and bladder [3]. It is present worldwide, but its incidence varies across countries and regions [4]. According to recent global and national epidemiological data, the marked increase in the occurrence of kidney stones in industrialized countries after the Second World War is associated with rising living standards and changes in dietary habits [5]. The high frequency of urolithiasis led scientists to try to understand how kidney stones

are formed, bearing in mind that about 80% of calcium oxalate stones are present in the pure form [6]. All kidney stones are in constant contact with extremely complex body fluids that have high ionic strength and contain biological macromolecules, small organic molecules and inorganic ions. Calcium oxalate stone formation may be a result of various metabolic disorders, such as hypercalciuria, hypocitraturia, hyperoxaluria or a change in urine acidity. The promotion and/or inhibition of oxalate stones is influenced by a wide range of compounds that can be found in urine, such as magnesium and citrate ions, organic micro- and macromolecules, glycosaminoglycans, etc. [7–10].

Calcium oxalates are sparingly soluble salts, which appear in the form of three hydrate modifications of different stability (solubility), namely monohydrate (COM), dihydrate (COD) and trihydrate (COT). COM is the most stable (the least soluble), while COT is the least stable and the most soluble. The most common hydrate form of calcium oxalate in kidney stones is COM, followed by COD [11]. Between these two hydrate forms, COM is more pathogenic as it can be found in the urine of people who are prone to urinary stone formation, while COD is physiologically more acceptable, as it can even be found in the urine of healthy people [12–14]. The formation of the respective hydrate forms, COM [15,16], COD [17–20] and COT [21,22], is influenced by several factors, such as the supersaturation, concentration, ratio of calcium to oxalate, presence of non-constituent components (additives), temperature, pH or method of mixing the reaction components [23–26]. Since the composition of urine, aside from calcium and oxalate ions, contains many other inorganic and organic molecules (regular physiological components or components that appear in pathological conditions), various studies have also been carried out under conditions as close as possible to those found in human urine [27–29] or in artificial urine [30,31]. The presence of significant quantities of inorganic and organic ions provides an average ionic strength of urine of about 0.33 mol dm^{-3}, while the pH varies from 4.5 to 9. Calcium and oxalate ions are always present at concentrations above the solubility product for COM. Typically, the major components of artificial urine, which is supposed to mimic the chemical composition of human urine, are urea, sodium and/or potassium chloride, sodium sulfate, magnesium sulfate, various sodium phosphate salts, sodium oxalate, calcium chloride and/or citrate (Table S1). As can be seen from Table S1, the composition of artificial urine, which can be adjusted to a certain type of research (precipitation of calcium oxalate monohydrate, dihydrate, phosphate, etc.), differs significantly [18,31–36]. Therefore, the results obtained in different model systems are difficult to compare. In 1980, Burns and Finlayson [31] proposed the chemical composition of the standard reference artificial urine. Nevertheless, recent research carried out in artificial urine continues to adapt the composition to specific experimental conditions and the desired goal [30].

Among the various organic molecules that can be found in urine, proteins should be highlighted, since they can often be incorporated into kidney stones. Consequently, all the α-amino acids (AAs) can be found in urinary stones, and the amino acids' content varies, depending on the physiological conditions during urolithiasis [37–39]. The effect of AAs on calcium oxalate hydrate precipitation has been studied by several researchers [40–44]. However, the literature data are contradictory, ranging from those showing an inhibition effect on precipitation [43] to the promotion of precipitation at low concentrations and inhibition at high concentrations [42]. Some authors found only slight or even no effect of high AA concentrations [40]. The addition of AAs has been observed to promote the formation of COM and prevent the formation of COD and COT [42], while other authors concluded that AA stimulates the formation of COD and inhibits COM [40]. It was also noted that some AAs (glutamic acid (Glu), glycine (Gly), lysine (Lys)) inhibit the nucleation process of COM, proline (Pro), alanine (Ala), valine (Val) or asparagine (Asn) promote the process, while serine (Ser) and phenylalanine (Phe) show just a minor effect on nucleation [45]. It is confirmed in the literature that the inhibition effect of certain AAs on the growth of COM crystals depends on their structure and that the effect is more pronounced with an increase in the AA concentration (Gly < Ala < Pro < aspartic acid (Asp) < Glu) [46]. Spontaneous precipitation of calcium oxalate from a solution of high ionic

strength (adjusted with NaCl) and with magnetic mixing, which promotes COT formation (either alone or in a mixture with COM), has also been investigated [21,22]. It has been shown that in such systems and by applying an AA such as Glu, tryptophan (Trp) or ornithine (Orn), the content of COT and COM in mixtures can be affected [41].

The mechanisms and conditions under which urinary stones are formed have not yet been fully clarified. Investigations of the spontaneous precipitation of calcium oxalates in the presence of different AAs under hyperoxaluria conditions have not been reported previously in the literature. Hyperoxaluria is a metabolic disorder of increased oxalate urine excretion. It contributes to the formation of stones by increasing the supersaturation of urine with respect to all the calcium oxalate hydrate phases. The disorder may occur as a primary or secondary hyperoxaluria [47]. It was found that in the systems with an increased concentration of oxalate, the formation of COM is favored [48,49]. In our previously reported study, we examined the calcium oxalate precipitation processes within a wide calcium and oxalate concentration range, which covers the conditions corresponding to hypercalciuria and hyperoxaluria [48]. In that work, chemically different model systems (MS) were investigated: (a) simple system—only calcium and oxalate reactants have been present, while in the (b) NaCl system—the ionic strength has been adjusted to physiological level by NaCl addition. Chemically, the most complex system was (c) the artificial urine. The results of our systematic study show that the molar concentrations, the supersaturations, the initial pH and the complexity of the system play an important role in the precipitation of calcium oxalate. The presence of NaCl and other inorganic ions in artificial urine stabilizes the metastable phase (COD) at higher relative supersaturation ranges.

The proposed study aims to distinguish the influence of system complexity and different AAs on calcium oxalate formation in these three precipitation systems with the increased concentration of oxalate ions, which mimics hyperoxaluria conditions. The selected AAs (Gly, Ala, Phe, His, Cys, Ser, Asp) have been found in the urine of healthy people, as well as in the urine of people susceptible to kidney stone formation. In conclusion, the addition of AAs does not affect the composition of the solid phase in the simple and NaCl systems but affects the composition in the artificial urine. The AAs affect the size of the COM crystallites, and the growth of the COM crystals increases with the increasing complexity of the system (simple < NaCl < artificial urine), and the AAs affect the morphology of the COM particles. Overall, polar amino acids and nonpolar Phe inhibit the growth of COM, which is the more pathogenic hydrate form and which can be found in the urine of people who are prone to kidney stone formation. Furthermore, the artificial urine system proved to be more relevant for the observation of effects relevant to kidney stone formation in the human body.

2. Materials and Methods

All the AAs used were α-AAs and were obtained from Sigma Aldrich, St. Louis, MO, USA. The AAs were classified according to their side chain groups: Ala, Phe (nonpolar), Gly, Ser, Cys (polar) and charged (His, Asp). The $CaCl_2$, $Na_2C_2O_4$ and NaCl (obtained from Sigma Aldrich, St. Louis, MO, USA) solutions were standardized by classical analytical volumetric methods. All the other chemicals used in the experiments were obtained from Sigma Aldrich (St. Louis, MO, USA). Ultra-pure water with a conductivity of less than 0.055 $\mu S\ cm^{-1}$ was used for the solution preparation.

2.1. Spontaneous Precipitation of Calcium Oxalate

The spontaneous precipitation experiments were carried out in three systems, which differed in terms of the chemical complexity:

(a) Simple system: composed of only the constituent ions (calcium and oxalate) and the respective counter ions (salts: $CaCl_2$ and $Na_2C_2O_4$).
(b) NaCl system: composed of the constituent ions (calcium and oxalate) and the respective counter ions and the sodium and chloride ions used to adjust the ionic strength to approximately 0.3 mol dm^{-3} (salts: $CaCl_2$, $Na_2C_2O_4$ and NaCl).

(c) Artificial urine system: composed of the constituent ions (calcium and oxalate) and the respective counter ions and other components that mimic the composition of the urine (Table S1). The artificial urine components were selected according to the protocol suggested by Burns and Finlayson [31] (salts: $CaCl_2$, $Na_2C_2O_4$, Na_2SO_4, KCl, NH_4Cl, NH_4OH, $MgSO_4 \cdot 7H_2O$ and NaCl). However, Na_2HPO_4 was excluded from the original protocol because phosphate salts can coprecipitate under the applied experimental conditions. In addition, the citrate ions, in the form of sodium citrate, have also been omitted, since it is known that they promote the formation of COD [20].

The initial pH value was adjusted to $pH_i = 5.0$ or $pH_i = 9.0$ by the addition of standardized HCl and/or NaOH solutions ($c = 0.01$ mol dm^{-3}). In all the systems, the initial concentration of calcium and oxalate was $c_i(Ca^{2+}) = 7.5$ mmol dm^{-3} and $c_i(C_2O_4{}^{2-}) = 6.0$ mmol dm^{-3}. The applied concentration range covers the hyperoxaluria conditions [47] in which kidney stones may be formed. The ionic strength of the systems was calculated according to the equation in the Supplementary Information. The initial supersaturation of the selected systems at both initial pHs ($pH_i = 5.00$ and 9.00) was as follows: S_i (simple system) ≈ 36, S_i (NaCl system) ≈ 24 and S_i (artificial urine) ≈ 21. Calculation of the initial supersaturation has been performed using the algorithm previously discussed in detail [48,50] or by VMINTEQ 3.1 (freely available at https://visual-minteq.software.informer.com/3.1/ accessed on 20 January 2023. The coordination of the oxalate ions with the calcium ions in the COM crystal was generated with the program MERCURY [51].

All the spontaneous precipitation experiments were carried out in a thermally insulated 400 cm^3 glass reaction vessel and the solution temperature was maintained at 37 °C. The vessel was closed using a Teflon stopper and the systems were mixed at 400–420 rpm with a PTFE-coated stirring bar on a magnetic mixer. The precipitation experiments were initiated by quickly pouring 200 cm^3 of oxalate solution into 200 cm^3 of calcium-containing solution. Appropriate amounts of the selected AAs were added each time to the oxalate solution before mixing with the calcium solution. The final concentration of the added AAs in all the systems was 30 mmol dm^{-3}.

The progress of the reaction was followed by measuring the pH of the solution using a combined glass/calomel electrode (HANNA Instruments HI1131, Woonsocket, RI, USA) connected to a digital pH meter (HANNA Instruments HI 5522, Woonsocket, RI, USA) connected to a computer. Once the approximately constant pH had been established, the experiment was stopped, the suspension was filtered through a 0.22 μm membrane filter (Millipore, Burlington, MA, USA), and the precipitate was washed with small amounts of deionized water and dried for one hour under a vacuum. All the experiments were performed in triplicate and the mean value is presented.

2.2. Experimental Methods

The precipitated calcium oxalates were characterized using Fourier transform infrared (FT-IR) spectroscopy, powder X-ray diffraction (PXRD), thermogravimetric analysis-differential scanning calorimetry (TGA-DSC), light microscopy (OM), and scanning electron microscopy (SEM). The IR spectra were recorded on a Shimadzu FTIR 8400S (Shimadzu Corp., Kyōto, Japan) spectrometer in the wavenumber range from 400 to 4000 cm^{-1} (resolution: 4 cm^{-1}). Diffuse reflectance infrared Fourier transformation (DRIFT) was also used: approximately 1 mg of solid sample was mixed with 100 mg of spectrometric grade KBr. IR Solution 1.30 software was used to record the spectra and process the data. The PXRD data were collected on a Rigaku Ultima IV diffractometer (Rigaku Holdings Corporation, Akishima-shi, Tokyo, Japan) using CuKα radiation in the 10–60° 2θ range at a scan rate of 1° min^{-1}. The COM modification was identified according to PDF card numbers 20-0231 and 75-1313, while the COD modification was identified based on PDF card number 17-541. The baselines of the PXRD patterns were corrected, and when needed, the data were smoothed using a 5-point Savitzky–Golay algorithm. The average crystallite size was estimated using the Debye–Scherrer method from the full width at half maximum of the 5 main reflections. The quantification of the phases was determined by the reference intensity ratio method.

The TGA-DSC analysis was carried out on a Mettler Toledo System 1 (Mettler Toledo, Columbus, OH, USA). The samples were tested in an oxygen atmosphere at a gas flow rate of 200 cm^3 min^{-1}, with a heating rate of 5 °C min^{-1} in a temperature range of 30 to 300 °C. The results were processed by STARe Software 10.0.

A light microscope (Orthoplan photographic microscope, E. Leitz, Leica, Wetzlar, Germany) and a scanning electron microscope, SEM (FESEM, JEOL JSM-7000F—JEOL, Akishima, Tokyo, Japan) were used for the visual identification of the precipitates and determination of the morphological properties of the precipitated phases.

3. Results

3.1. Spontaneous Precipitation of Calcium Oxalate in the Systems with the Addition of Amino Acids

In our presented research, we used three types of systems with different complexities: (a) only calcium and oxalate ions (simple system), (b) increased ionic strength by the addition of NaCl (NaCl system) and (c) artificial urine at two initial pHs (pHi = 5.0 and 9.0). The ionic strength of these systems increased from system (a) to system (c), and with it, the supersaturation decreased. The supersaturation is one of the crucial parameters that define the precipitation of sparingly soluble substances. A decrease in supersaturation indicates a decrease in the nucleation rate, which might lead to the formation of the precipitates/crystals with different properties (for example, the formation of the crystals with the different morphology or change in the composition of the precipitate). The aim of this work was to investigate how the complexity of the system, as reflected by changes in the ionic composition, influences the precipitation of calcium oxalate, particularly in the context of the addition of amino acids.

3.1.1. FTIR and PXRD Characterization of Precipitates

The influence of AAs on calcium oxalate's spontaneous precipitation was studied in the simple system, NaCl system and artificial urine with $c_i(C_2O_4^{2-})$ = 6.0 mmol dm^{-3} and $c_i(Ca^{2+})$ = 7.5 mmol dm^{-3}. The characterization of the precipitates was performed by FTIR and PXRD analysis. FTIR was mainly used for the qualitative determination of oxalate hydrates in the samples, while the quantitative proportion of oxalate hydrates was determined using powder diffraction. Additionally, the TGA method was only performed on the model systems (MS) and obtained results correspond to the literature data (Table S2) [48,52].

Figures 1–3 show the IR spectra and PXRD diffractograms of the oxalates obtained by spontaneous precipitation in the AA-containing systems.

The obtained IR and PXRD results, as shown in Figure 1A,B, were compared with the oxalate standards (COM and COD) provided in Table S3 and Figure S4 in the Supplementary Information. The analyses indicated that the formation of the specific hydrate phase is not affected by the addition of AAs, since only the COM phase was detected in all the systems. The TGA analysis of the MS also confirmed the precipitation of only COM (Table S2).

Similarly to the simple system, regardless of the addition of AAs in the NaCl system (Figures 2 and S4, Tables S2 and S3), the composition of the hydrated phase does not change and the most stable form, COM, precipitates.

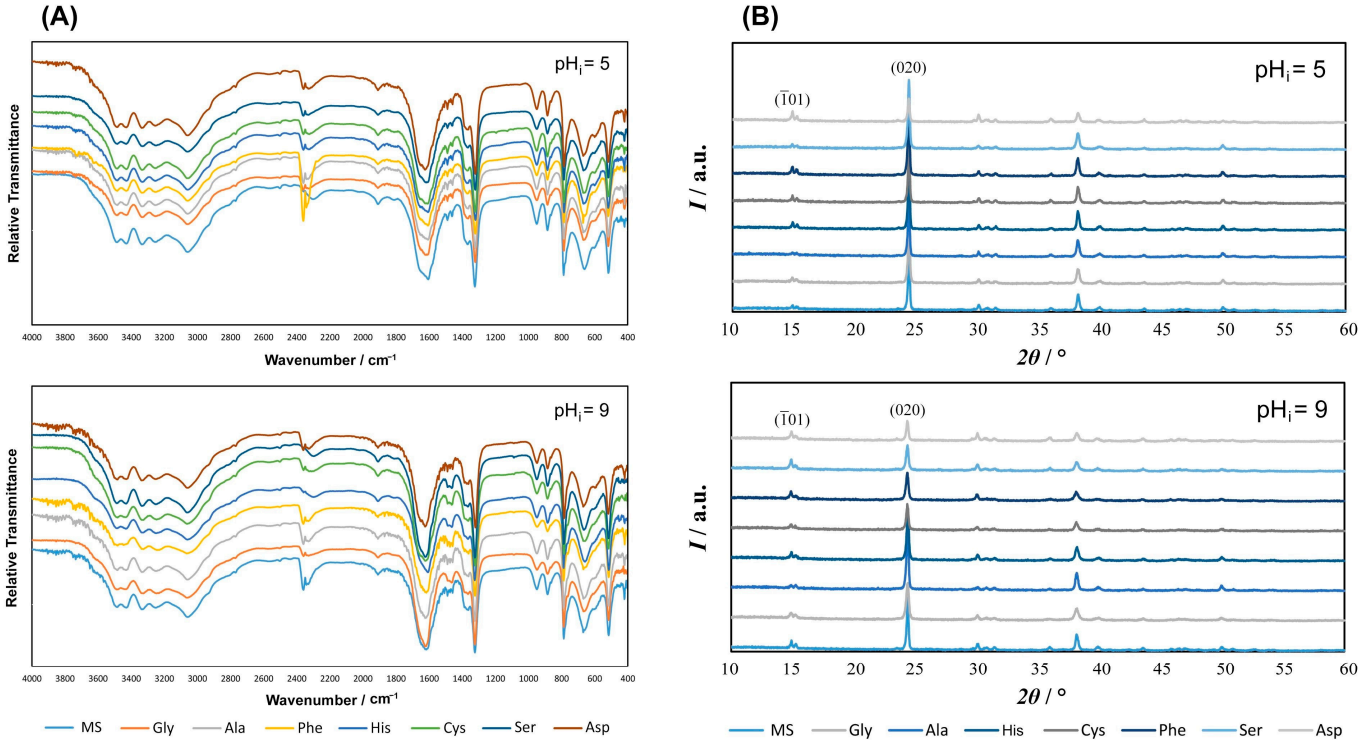

Figure 1. (**A**) IR spectra and (**B**) PXRD diffractograms of samples precipitated in a simple system at pH_i = 5.0 and pH_i = 9.0 with the addition of AAs. MS—model system, Gly—glycine, Ala—alanine, Phe—phenylalanine, His—histidine, Cys—cysteine, Ser—serine, Asp—aspartic acid.

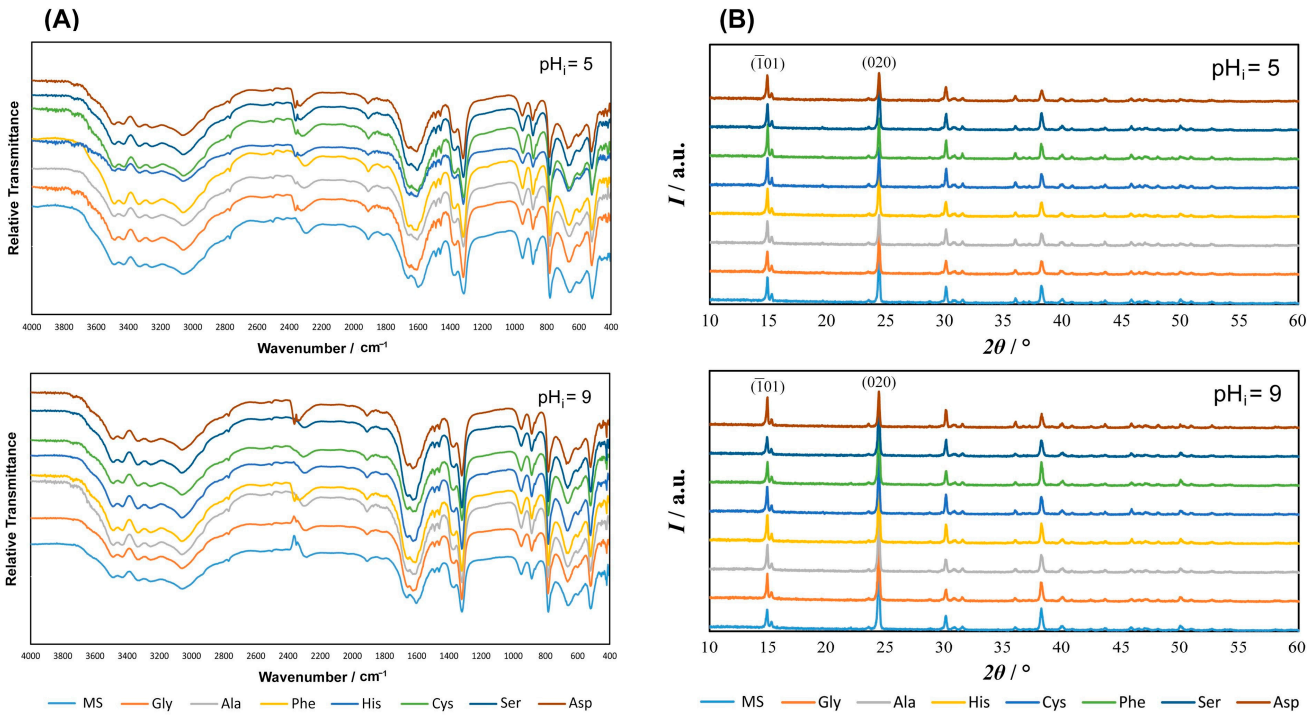

Figure 2. (**A**) IR spectra and (**B**) PXRD diffractograms of samples precipitated in the NaCl system at pH_i = 5 and pH_i = 9 with the addition of AAs. MS—model system, Gly—glycine, Ala—alanine, Phe—phenylalanine, His—histidine, Cys—cysteine, Ser—serine, Asp—aspartic acid.

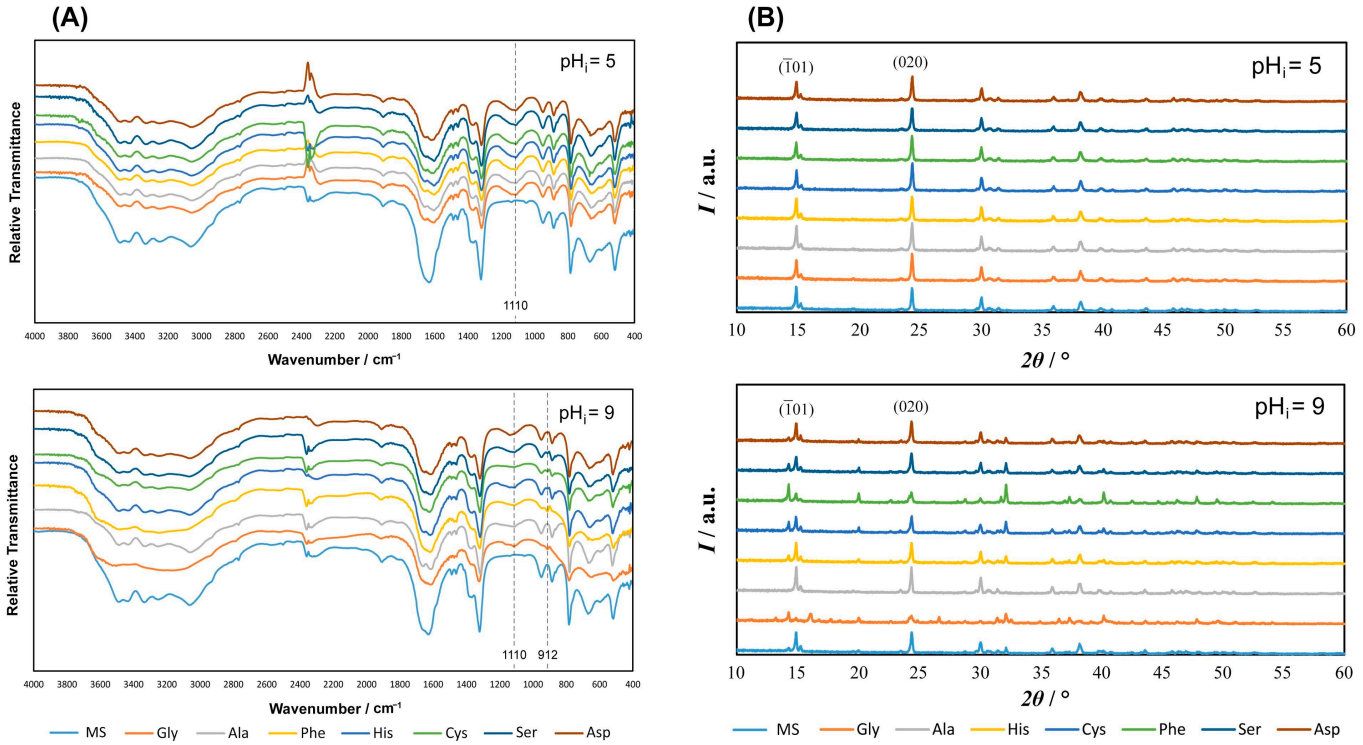

Figure 3. (**A**) IR spectra and (**B**) PXRD diffractograms of samples precipitated in the artificial urine system at pH_i = 5.0 and pH_i = 9.0 with the addition of AAs. MS—model system, Gly—glycine, Ala—alanine, Phe—phenylalanine, His—histidine, Cys—cysteine, Ser—serine, Asp—aspartic acid.

Figure 3A shows the IR spectra of the precipitated calcium oxalates in artificial urine with the addition of AAs. In all the systems at pH_i = 5.0, only COM precipitated, but a significant change occurred in the systems at pH_i = 9.0, in which the COM/COD mixture precipitated. Compared to the model system (MS—system without AA), a vibration band at approximately 1110 cm^{-1} appeared, which corresponds to a vibration of the C−OH, thus indicating that AAs can be integrated into crystalline aggregates or can be adsorbed on the crystal surfaces [53,54]. In the model systems at both pH_i, in the vibrational range above 3000 cm^{-1}, five sharp bands were visible, which correspond to the antisymmetric and symmetric stretching of coordinated water molecules (Table S3). In the systems with AAs, the indicated area is wider and the sharp bands are less prominent [17,55]. These changes can be caused by the complex hydrogen bonds between C=O groups in $C_2O_4^{2-}$ and H_2O, $-NH_2$ or −COOH functional groups in AAs [54]. In the samples prepared with Gly, Phe, Cys and Ser at pH_i = 9.0, a vibration band was observed at approximately 912 cm^{-1}, indicating the greater amount of the COD modification (Table S3, Figure S4). The other spectra were specific to COM (Table S3, Figure S4).

To determine the content of each hydrate phase, a quantitative analysis was carried out based on PXRD (Figure 4).

All the AAs at pH_i = 9.0 are in anionic form and they bind through electrostatic interactions to COM [56]. Therefore, the polar AAs (with the polarity increasing in the sequence Gly > Cys > Ser) had a more significant impact on the inhibition of COM formation, enabling greater growth of COD. In addition to the polar AAs, the inhibition of COM was also significantly influenced by Phe.

Figure 5 shows the impact of amino acids on the COM crystallite size. The size of the COM crystallite precipitated in the absence of AAs at both pH_i is as follows: 54 ± 4 nm in the simple system, 56 ± 3 nm in the NaCl system and 55 ± 5 nm in artificial urine.

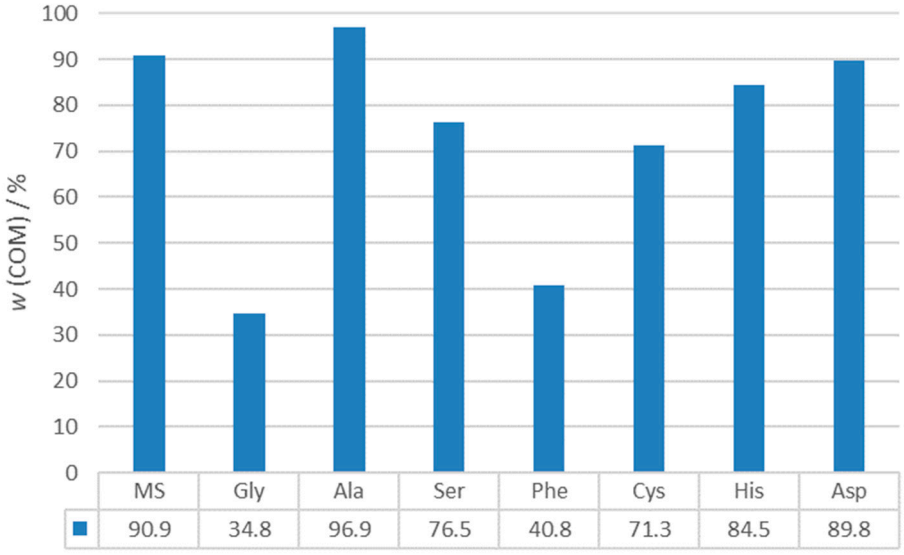

Figure 4. The content ($wt/\%$) of precipitated COM in artificial urine containing different AAs and at pH_i = 9.0. MS—model system, Gly—glycine, Ala—alanine, Phe—phenylalanine, His—histidine, Cys—cysteine, Ser—serine, Asp—aspartic acid.

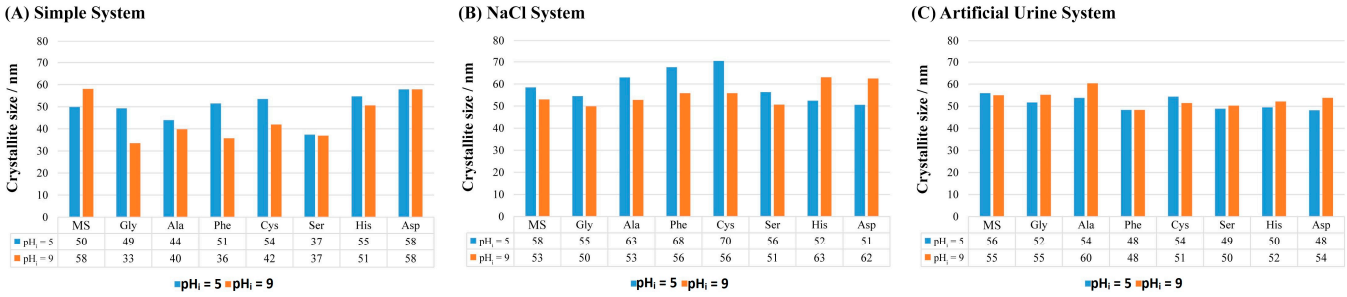

Figure 5. Influence of AAs on the crystallite size of COM in different systems. MS—model system, Gly—glycine, Ala—alanine, Phe—phenylalanine, His—histidine, Cys—cysteine, Ser—serine, Asp—aspartic acid. (**A**) Simple System (**B**) NaCl System (**C**) Artificial Urine System.

The greatest effects of AA addition on the COM crystallite size were recorded at pH_i = 9.0 in the simple systems containing nonpolar (Ala, Phe) and polar (Gly, Ser, Cys) AAs, in which significantly smaller crystallites (33–42 nm) were obtained. At pH_i = 5, smaller crystallites (37 and 44 nm) were also observed with the addition of Ser and Ala. No significant changes in the crystallite size were noticed in the artificial urine system.

3.1.2. SEM Characterization of Precipitates

The morphology of the COM in the simple systems at pH_i = 5.0 and pH_i = 9.0 was studied with light and SEM microscopy (Figure 6). The SEM images demonstrated morphology differences in the surface texture and crystal edges. It was observed that the particles formed at pH_i = 5.0 have a flat and smooth surface with rounded edges. Compared to this texture, the COM dendritic particles formed at pH_i = 9.0 are composed of cubic and/or elongated primary crystallites with more or less "protruding" crystallites, which have wrinkled and porous surfaces with jagged edges.

The addition of AAs to the systems influenced the morphology, size and texture of the COM dendritic particles. The light microscope images of the COM particles in the systems with AA addition show that the individual crystals are more branched at pH_i = 5.0 (except Asp) and remain larger compared to the crystals obtained at pH_i = 9.0.

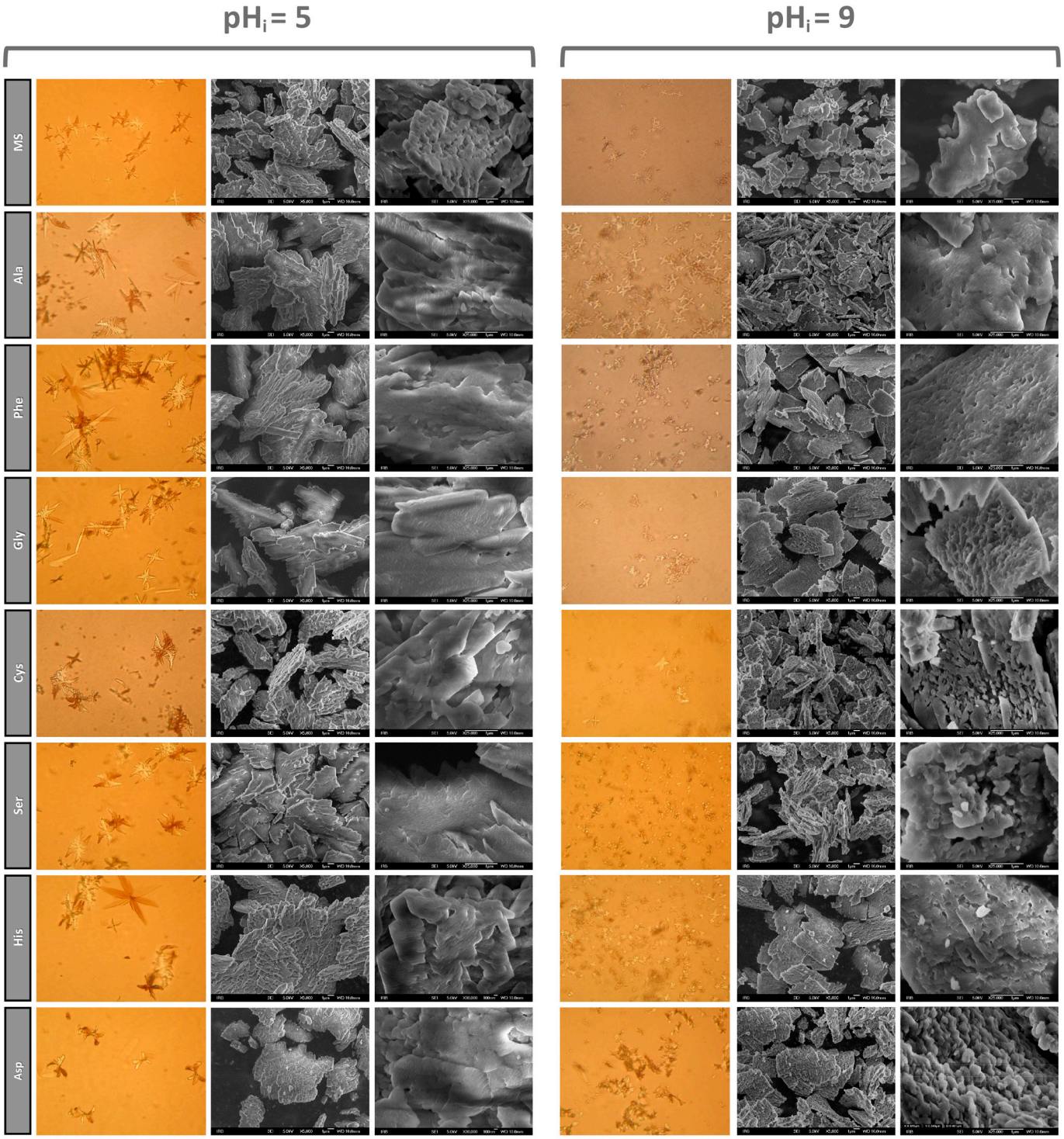

Figure 6. Light microscope and SEM images of calcium oxalate samples in a simple system with AAs at pH$_i$ = 5.0 and pH$_i$ = 9.0. MS—model system, Gly—glycine, Ala—alanine, Phe—phenylalanine, His—histidine, Cys—cysteine, Ser—serine, Asp—aspartic acid.

The morphology of the COM crystals precipitated in the NaCl systems at pH$_i$ = 5.0 and pH$_i$ = 9.0 is shown in Figure 7. In the model system, more or less platelet-shaped COM particles were formed, with visible dendritic structures and aggregated smaller particles. The decrease in the amount of the dendritic structure and the increase in the particle content can be associated with a significant decrease in supersaturation ($S_i \approx 24$) compared to the simple system ($S_i \approx 36$) and aggregation may be associated with the increase in the ionic

strength [57]. The SEM images show a difference in the texture of the surfaces and edges of these particles.

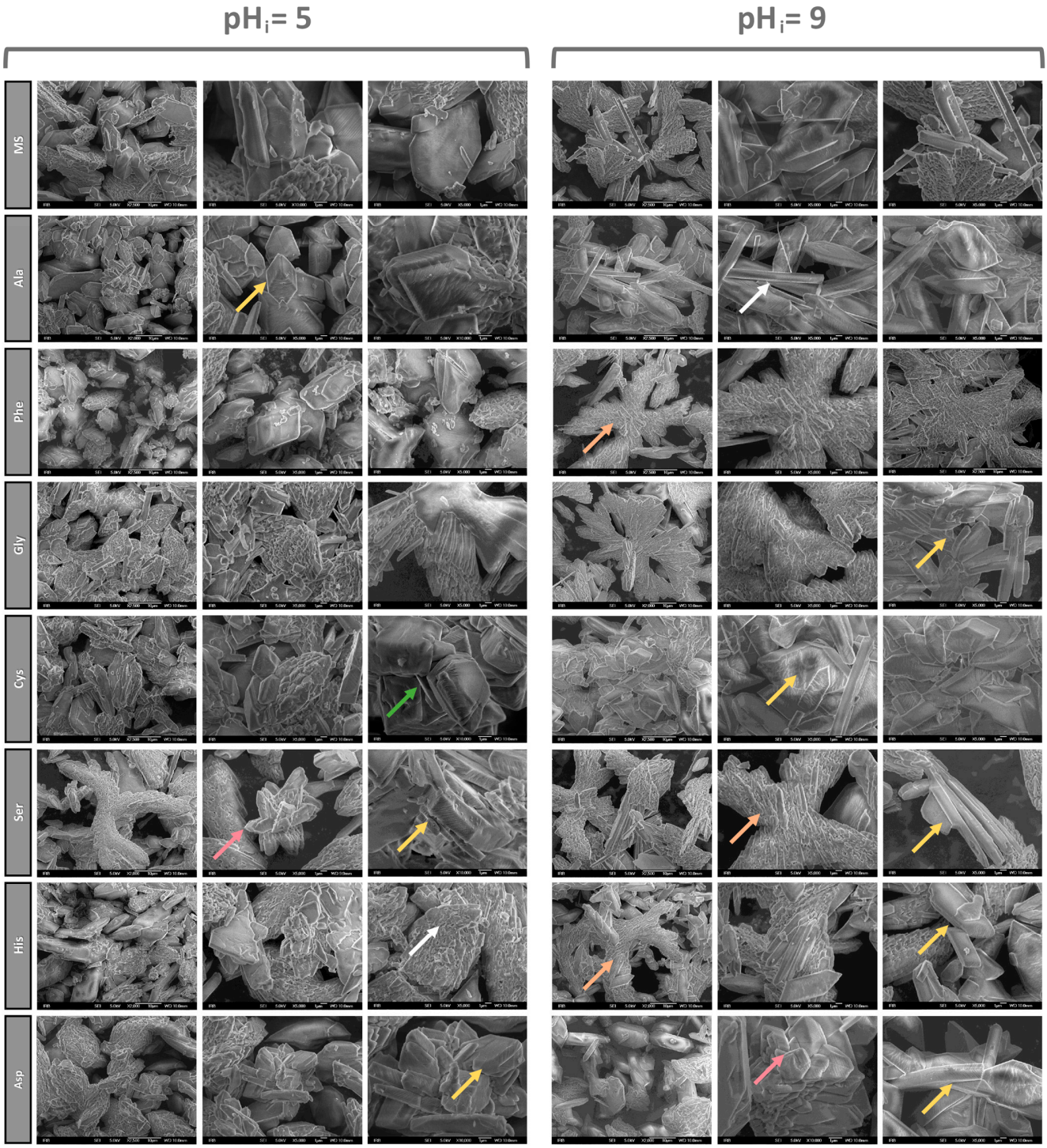

Figure 7. SEM images of calcium oxalate samples precipitated in the NaCl system with the addition of different AAs at pH_i = 5.0 and pH_i = 9.0. Yellow and white arrows mark COM of different habitus. Orange arrows show a dendritic structure. Pink arrows show growth in COM and green arrows aggregation. MS—model system, Gly—glycine, Ala—alanine, Phe—phenylalanine, His—histidine, Cys—cysteine, Ser—serine, Asp—aspartic acid.

It was observed that the platelet-shaped particles formed at pH_i = 5.0 have smoother surfaces, rounded edges and more densely and regularly distributed surface furrows. In

the model system, more or less platelet-shaped COM particles were formed, with visible dendritic structures and aggregated smaller particles. Compared to this, the COM particles formed at pH_i = 9.0 exhibited a flat and smooth surface with sharper edges. The dendritic plates were significantly smaller compared to the simple system and the crystals exhibited a more or less regular hexagonal shape. After AA addition to the systems, a more significant effect on the morphology of the COM dendritic particles was observed. In the case of Phe, Ser and His at pH_i = 9.0, the effect of stabilizing the dendritic structure was observed (Figure 7—orange arrows). The effect of aggregation was more or less present in all the systems (Figure 7—green arrows).

The morphology of the solid phase obtained by spontaneous precipitation of calcium oxalate in artificial urine at both pH_i is shown in Figure 8. In the model system, more or less plated COM particles without a visible dendritic structure were formed, along with strongly aggregated smaller particles. The disappearance of the dendritic particles and the increase in the amount of more or less regular particles compared to the NaCl system can be linked to the fact that the artificial urine system is a slightly less saturated system ($S_i \approx 21$) compared to the NaCl system ($S_i \approx 24$). This created the conditions for an even more significant reduction in the initial supersaturation compared to the simple system ($S_i \approx 36$), thus inhibiting the dendritic growth of crystals. The SEM images showed a difference in the texture of the surfaces and edges of these particles. The COM crystals formed at pH_i = 5.0 had smooth surfaces, as in the two previous systems, and their edges were rounded. In comparison to this texture, the COM particles precipitated at pH_i = 9.0 also showed a smooth surface, alongside stacks of elongated primary crystals with more or less "protruding" crystallites with a folded surface and porosity effect.

The crystals in the model systems assume a regular hexagonal shape with well-developed (020) and (021) faces, as reported in the literature [58,59]. Morphology of COM crystals with characteristic Miller indices and the coordination of oxalate ions with calcium ions in COM crystals is shown on Figure S3. The addition of the AAs to the systems caused significant changes in the COM morphology. The aggregation effect is present in all the systems (Figure 8—green arrows). The growth effects of COM are marked with pink arrows. Two types of growth are visible. In the first, growth starts on the pre-created steps and spreads uniformly along the whole face (for example, Ser at both pH_i), while in the other case, the growth starts at several sources on the same face (for example, Phe at pH_i = 5). The result of the growth of COM crystals (yellow and white arrows) is observed as a change of habitus, i.e., by the twisting and rounding of the COM particles. Also, the apparent growth in height (loss of the plate structure) or the development of plate-like COM particles can be observed. The platelets of the COM crystals in some systems are compact aggregates of smaller crystallites that stack up regularly (orange arrow).

Pink arrows indicate the growth effects of COM. Growth starts on the previously created steps and extends along the whole $(\bar{1}01)$ face. The various habitus of the COM crystals resulting from the growth of crystals are marked by yellow and white arrows. Yellow arrows show the thickening and rounding of the COM particles and their apparent growth in height (the plate structure is lost), while white arrows show the existence of plate-like COM particles.

Unlike in the two previous systems, the artificial urine system promotes COD precipitation at pH_i = 9.0 (blue arrows) for the AAs Phe, Gly, Cys and Ser. The systems with other AAs contained lower amounts of COD at pH_i = 9.0.

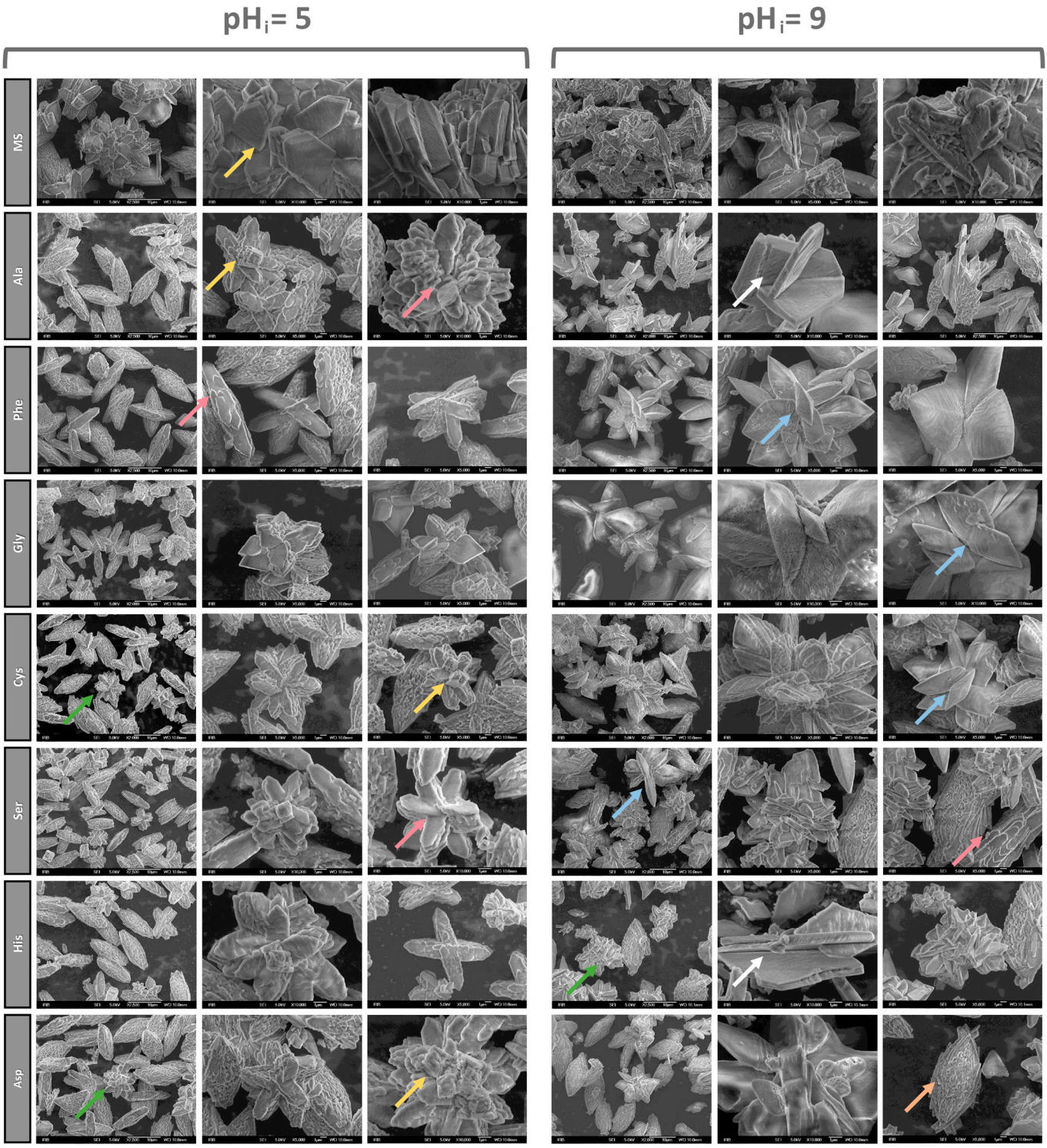

Figure 8. SEM images of calcium oxalate samples precipitated in artificial urine with the addition of different AAs at pH_i = 5.0 and pH_i = 9.0. Blue arrows show COD crystals, while yellow and white arrows show COM particles of different habitus. The orange arrow displays an aggregate plate structure. Pink arrows show growth in COM and green arrows aggregation. MS—model system, Gly—glycine, Ala—alanine, Phe—phenylalanine, His—histidine, Cys—cysteine, Ser—serine, Asp—aspartic acid.

The literature data show that the AAs in the urine can be adsorbed onto the calcium oxalate crystal surfaces, thus affecting their growth, aggregation and transformation [60].

Depending on the AAs' ionic form in the solution, they can bind to Ca^{2+} and/or $C_2O_4^{2-}$ on the crystal surface of calcium oxalate. Carboxylic acids and their salts are known to be growth inhibitors [61], while as a result of electrostatic interaction with surfaces, significant changes in morphology can be expected [62]. Another issue that is insufficiently studied is the effect of additives, especially organic ones, on the process of aggregation, which typically occurs during the final stages of the crystallization/precipitation process. Indeed, the literature findings are contradictory: some authors claimed that organic compounds act as an adhesive that facilitates the aggregation of the resulting crystals [21], while others claimed that organic additives prevent aggregation [63]. Therefore, the impact of organic additives like AAs on aggregation, which is thought to be essential for understanding lithogenesis mechanisms, requires further investigation. We found that in the NaCl system, regardless of the addition of AAs, the beginning of aggregation could be observed, while in the artificial urine system, more pronounced aggregation occurs regardless of the addition of AAs. Therefore, it can be concluded that the chemical complexity of the system in which calcium oxalates precipitated has a significant influence on the aggregation. Overall, the difference in the composition, morphology, and extent of the crystal aggregation in all three systems demonstrates that the artificial urine system is more relevant since it is more similar to the conditions in the human body. The simple system and the complex NaCl system are not optimal for the observation of changes in the calcium oxalates on a broader scale, but they can be used to determine the influence of individual components of urine. However, the simple and NaCl system will not provide information on the overall effects relevant to kidney stone formation in the human body.

3.1.3. Effect of Amino Acids on the Habitus of COM Crystals

The main exposed faces of the COM crystals are the ($\bar{1}$01), (020), ($\bar{2}$02), and (130) planes (Figures S3 and S4). Many authors demonstrated that the growth of specific crystal planes is reflected in the higher intensity of the corresponding diffraction peak in the samples' diffractogram. Namely, crystal growth of the (020) plane caused a more intense (020) reflection in the PXRD pattern. By contrast, the crystal growth of the ($\bar{1}$01) plane caused an increased ($\bar{1}$01) reflection in the PXRD pattern. The changes in the (020) and ($\bar{1}$01) planes can often be observed in the morphology of the precipitated crystal, where the (020) face or the ($\bar{1}$01) face of the COM crystals is more pronounced, respectively [57,64–67].

In ($\bar{1}$01) (Figure S3B), the surface layer planes contain two sub-layers of oxalate groups; one is parallel and the other is perpendicular to the plane. Groups of oxalates on the plane lie below the top surface layer (not 'strip') and such a structure makes the plane rich in Ca^{2+} ions [40,54,67], while the (020) plane is characterized by the oxalate ions lying perpendicular to the face, alternating with those parallel to the face. The ($\bar{1}$01) plane has the highest densities of calcium ions on the surface (0.54 $Ca^{2+}/Å^2$) and, as a result, favorably binds the more negative molecule/ion [68].

The ratios of the intensity of the ($\bar{1}$01) and (020) PXRD peaks were determined, and the results are presented in Table 1. The intensity ratio I ($\bar{1}$01)/I (020) observed in all the model systems at both pH_i gradually increased from the simple via the NaCl to the artificial urine system (in Table 1 marked as A. urine): at pH_i = 5.0: 0.1178 < 0.4474 < 1.0649 and at pH_i = 9.0: 0.2078 < 0.2662 < 1.0041. These results indicate that in the model systems with increasing system complexity, the intensity of the ($\bar{1}$01) reflection increases as a result of the more pronounced ($\bar{1}$01) faces in the calcium oxalate crystals.

At pH_i = 5.0, all the AAs are mostly in the form of zwitterions (except the charged AAs), and there are two possible interactions: interaction of the positive part of the AA (protonated amino groups) with the negative part of the COM crystal ($C_2O_4^{2-}$) or interactions of the negative part of the AA (deprotonated carboxyl groups) with the positive part of the COM crystal (Ca^{2+}). At pH_i = 9.0, the AAs are mostly in the anionic form and are preferentially bound by their negative part (deprotonated carboxyl group) to the positive part of the COM crystal (Ca^{2+}).

Table 1. The intensity ratio I ($\bar{1}01$)/I (020). A. urine—artificial urine system.

		pH_i = 5			pH_i = 9		
I ($\bar{1}01$)/I (020)		**Simple**	**NaCl**	**A. urine**	**Simple**	**NaCl**	**A. urine**
Non-polar AA	Model	0.1178	0.4474	1.0649	0.2078	0.2662	1.0041
	Ala	0.0890	0.8042	0.8620	0.0885	0.4025	0.9759
	Phe	0.1349	0.6878	0.6708	0.3613	0.2219	0.9275
Polar AA	Gly	0.0910	0.5625	0.7300	0.2218	0.3646	0.7365
	Ser	0.0775	0.4726	0.7182	0.5370	0.3318	0.8276
	Cys	0.1061	0.7374	0.6341	0.3220	0.4628	0.9326
Charged AA	His	0.1185	0.6063	0.9132	0.2176	0.3789	1.0212
	Asp	0.4391	0.9248	0.7643	0.5425	0.7634	0.9126

In the simple and NaCl systems, an increase in the ratio of I ($\bar{1}01$)/I (020) was observed for most of the examined AAs, with this effect being more pronounced in the NaCl system at both pH_i values. The most pronounced effect was observed in the case of Asp, which can be attributed to the presence of a side-charged group, which Asp possesses alongside the main groups (amino and carboxyl) present in all the AAs. This additional charged group enables Asp to have a stronger interaction with the COM surface. The observed effect of the increase in the ratio indicates the promotion of the growth of the ($\bar{1}01$) plane.

In the artificial urine, a decrease in the ratio of I ($\bar{1}01$)/I (020) was obtained, and this effect was more pronounced at pH_i 5.0 for all the AAs. In the artificial urine, numerous different ions can interact with the main and side groups of AAs, which are in the form of zwitterions at pH_i = 5.0, having two charged groups for interaction. As a result of these interactions between the AAs and ions in the artificial urine, as well as the interactions between the AAs and the COM surface, the growth of the (020) plane becomes more pronounced. The most pronounced effects of decreasing the ratio were observed at both pH_i values in the presence of the polar AAs and Phe.

The noted effects are consistent with observations found in the literature. Shen et al. [53,54] investigated the influence of Asp, Tyr and Trp on the precipitation of calcium oxalate and concluded that the pH of the system and the increase in the AA concentration affect the intensity ratio I (020)/I ($\bar{1}01$). When the pH is higher than the isoelectric points of the AA under consideration, the intensity ratio becomes gradually smaller and COM growth parallel to the ($\bar{1}01$) plane is more favored. When the pH is lower than the isoelectric points of the AA (such as for Trp), an excess of positive charges are present on the surface, and they attracting more oxalate ions, which results in crystal growth parallel to the (020) face. Consequently, the measured value of I (020)/I ($\bar{1}01$) is higher.

4. Conclusions

Precipitation experiments of calcium oxalates under the conditions typical of hyperoxaluria ($c_i(Ca^{2+})$ = 7.5 mmol dm^{-3} and $c_i(C_2O_4{}^{2-})$ = 6.0 mmol dm^{-3}) and the addition of selected AAs (Ala, Phe, Gly, Cys, Ser, His, Asp; c = 30 mmol dm^{-3}) have been performed in systems of different chemical complexity: simple system, NaCl and artificial urine system, at pH_i = 5.0 and pH_i = 9.0. The results indicated the following:

1. The addition of AAs does not affect the composition of the solid phase in the simple and NaCl systems but shows an effect in the artificial urine. In the simple and NaCl systems at both pH_i, and the artificial urine at pH_i = 5.0, only COM precipitated. In the artificial urine at pH_i = 9.0, the formation of COD was observed. The maximum content of COD was obtained in the systems with the addition of polar AAs and Phe (w(COD): Gly 65.2 % > Phe 59.2 % > Cys 28.7 % > Ser 23.5%). The effect can be explained by the fact that all the AAs at pH_i = 9.0 were in the anionic form, so the electrostatic interactions of the AAs with the COM crystals, complemented by the additional hydrogen bonding of the side chains, inhibit its growth and consequently promote COD formation.

2. The addition of AAs affects the size of the COM crystallites and the most significant impact was in the simple system. In the artificial urine system, the addition of AAs did not significantly affect the crystallite size.
3. The addition of AAs affects the growth of COM crystals in all the investigated systems (simple, NaCl and artificial urine) at both pH_i. The most pronounced effect in the simple and NaCl systems was observed in the case of Asp, which can be attributed to the presence of a side-charged group and stronger interaction with the COM surface. In the artificial urine, the most pronounced effects were in the presence of the polar AAs and Phe, where the growth of the (020) plane was promoted.
4. In the NaCl and artificial urine systems, crystal aggregation was observed. The AAs affect the morphology of the COM particles, so at pH_i = 5.0 in all the systems, the COM crystals have relatively smooth surfaces but their edges are rounded, stacked and regularly distributed. The combination of AAs and pH_i = 9.0 gave rise to a porous structure on the COM crystal surfaces that is visualized as a slide of elongated primary crystals with roughly "protruding" crystallites.

In all the systems, the amino acids have the greatest influence on the morphology of the obtained calcium oxalate precipitates. Overall, the difference in the composition, morphology, and extent of the crystal aggregation in all three systems demonstrates that the artificial urine system is more relevant since it is more similar to the conditions in the human body. Based on the results of the structural and morphological analyses of the precipitates, it is possible to assess the role of the chemical complexity of the precipitation system, as well as the mode of interaction (promotion or inhibition) of the selected AAs with specific calcium oxalate hydrate phases under conditions that simulate hyperoxaluria in the urinary system. It can also be assumed that most of the observed amino acids can act as potential inhibitors of the precipitation of the pathogenic form of calcium oxalate (COM) under certain conditions. Future research in this area should certainly also investigate the influence of the aforementioned amino acids, COM and COD on cell lines.

Supplementary Materials: The following supporting information can be downloaded at https://www.mdpi.com/article/10.3390/cryst14070599/s1, Materials and Methods—ionic strength calculation; Table S1. Composition of artificial urine from the literature sources [18,31–36]; Table S2. Thermogravimetric analyses of the model system (MS) ($c(C_2O_4^{2-})$ = 6.0 mmol dm^{-3} and $c(Ca^{2+})$ = 7.5 mmol dm^{-3}) in a simple system, NaCl system and artificial urine at pH_i = 5 and pH_i = 9 (t_0—initial temperature, t_{max}—maximum temperature, t_e—end temperature, Δm—mass loss expressed as a percentage, hydrate form that precipitates) [48,52]; Figure S1. (A) IR spectra of samples prepared in the model system at pH_i = 5 and pH_i = 9, and (B) diffractograms of samples prepared in the model system at pH_i = 5 and pH_i = 9 (blue arrows indicate diffraction maxima from COD) [48]; Figure S2. Light microscope images (a) and SEM images (b) of calcium oxalate precipitated in the model systems (systems without AAs) at pH_i = 5 and pH_i = 9. Note the difference in the SEM scale (×5.000, ×2.500) [48]; Figure S3. (A) Morphology of COM crystals with characteristic Miller indices and crystal growth direction (black numbers correspond to Tazzoli notation (space group $P2_1/c$) [58] and red to Deganello notation (space group $I2/m$)) [59], and (B) The coordination of the oxalate ions with the calcium ions in the COM crystal, drawn with the program MERCURY [51]; Figure S4. PXRD diffractograms of the standards: (a) COM (black-marked planes according to PDF card 75-1313, red-marked planes according to PDF card 20-231) and (b) COD (black-marked planes according to PDF card 17-541 for COD); Table S3. IR vibration bands (in cm^{-1}) of the calcium oxalate standards COM and COD [17].

Author Contributions: Conceptualization, A.S., N.M.M. and J.K.; methodology, A.S., N.M.M., J.K. and B.Nj.Dž.; software, B.Nj.Dž.; validation, B.Nj.Dž.; formal analysis, A.S.; investigation, A.S., D.M.L. and J.K.; resources, B.M. and D.K.; data curation, A.S.; writing—original draft preparation, A.S., N.M.M., J.K., D.K., B.M. and B.Nj.Dž. writing—review and editing, A.S., N.M.M., D.M.L., J.K. and B.Nj.Dž.; visualization, A.S.; supervision, A.S. All authors have read and agreed to the published version of the manuscript.

Funding: This research received no external funding.

Data Availability Statement: The data that support the findings of this study are available from the corresponding authors upon reasonable request.

Conflicts of Interest: The authors declare no conflicts of interest.

References

1. Campodoni, E.; Montanari, M.; Artusi, C.; Bassi, G.; Furlani, F.; Montesi, M.; Panseri, S.; Sandri, M.; Tampieri, A. Calcium-Based Biomineralization: A Smart Approach for the Design of Novel Multifunctional Hybrid Materials. *J. Compos. Sci.* **2021**, *5*, 278. [CrossRef]
2. Scotland, K.B.; Wong, G.C.; Matusik, K.; Lun, M.C.; Gul, S.; Su, F.; Vine, D.; Gelb, J.; Yun, W. Understanding 3D Biomineralization in Human Kidney Stones with Correlative X-ray Micro-CT & X-ray Fluorescence Microscopy. *Microsc. Microanal.* **2022**, *28*, 288–289. [CrossRef]
3. Tsolaki, E.; Bertazzo, S. Pathological Mineralization: The Potential of Mineralomics. *Materials* **2019**, *12*, 3126. [CrossRef] [PubMed] [PubMed Central]
4. Ferraro, P.M.; Bargagli, M.; Trinchieri, A.; Gambaro, G. Risk of Kidney Stones: Influence of Dietary Factors, Dietary Patterns, and Vegetarian-Vegan Diets. *Nutrients* **2020**, *112*, 779. [CrossRef] [PubMed] [PubMed Central]
5. Coello, I.; Sanchis, P.; Pieras, E.C.; Grases, F. Diet in Different Calcium Oxalate Kidney Stones. *Nutrients* **2023**, *15*, 2607. [CrossRef]
6. Chen, T.; Qian, B.; Zou, J.; Luo, P.; Zou, J.; Li, W.; Chen, Q.; Zheng, L. Oxalate as a potent promoter of kidney stone formation. *Front. Med.* **2023**, *10*, 1159616. [CrossRef] [PubMed]
7. Wang, Z.; Zhang, Y.; Zhang, J.; Deng, Q.; Liang, H. Recent advances on the mechanisms of kidney stone formation (Review). *Int. J. Molec. Medic.* **2021**, *48*, 149. [CrossRef]
8. Alelign, T.; Petros, B. Kidney Stone Disease: An Update on Current Concepts. *Adv. Urol.* **2018**, *2018*, 3068365. [CrossRef]
9. Ruiz-Agudo, E.; Burgos-Cara, A.; Ruiz-Agudo, C.; Ibañez-Velasco, A.; Cölfen, H.; Rodriguez-Navarro, C. A non-classical view on calcium oxalate precipitation and the role of citrate. *Nat. Commun.* **2017**, *8*, 768. [CrossRef]
10. Kumar, V.; Lieske, J.C. Protein regulation of intrarenal crystallization. *Curr. Opin. Nephrol. Hypertens.* **2006**, *15*, 374–380. [CrossRef]
11. Schubert, G. Stone analysis. *Urol. Res.* **2006**, *34*, 146–150. [CrossRef] [PubMed]
12. Anderegg, M.A.; Olinger, E.G.; Bargagli, M.; Geraghty, R.; Taylor, L.; Nater, A.; Bruggmann, R.; Sayer, J.A.; Vogt, B.; Schaller, A.; et al. Prevalence and characteristics of genetic disease in adult kidney stone formers. *Nephrol. Dial. Transplant.* **2024**, gfae074. [CrossRef] [PubMed]
13. Sharma, S.; Sharma, N.N.; Chandra Gupta, P.; Verma, R.; Yadav, V. An Update on Kidney Stones: Types, Mechanism and Treatment Approaches. *Res. J. Pharmacogn. Phytochem.* **2023**, *15*, 53–62. [CrossRef]
14. Vinaiphat, A.; Thongboonkerd, V. Prospects for proteomics in kidney stone disease. *Expert. Rev. Proteom.* **2017**, *14*, 185–187. [CrossRef] [PubMed]
15. Bramley, A.S.; Hounslow, M.J.; Ryall, R.L. Aggregation during precipitation from solution. Kinetics for calcium oxalate monohydrate. *Chem. Eng. Sci.* **1997**, *52*, 747–757. [CrossRef]
16. Pitt, K.; Mitchell, G.P.; Ray, A.; Heywood, B.R.; Hounslow, M.J. Micro-mechanical model of calcium oxalate monohydrate aggregation in supersaturated solutions: Effect of crystal form and seed concentration. *J. Cryst. Growth* **2012**, *361*, 176–188. [CrossRef]
17. Conti, C.; Casati, M.; Colombo, C.; Realini, M.; Brambilla, L.; Zerbi, G. Phase transformation of calcium oxalate dihydrate—Monohydrate: Effects of relative humidity and new spectroscopic data. *Spectrochim. Acta Part A Mol. Biomol. Spectrosc.* **2014**, *128*, 413–419. [CrossRef] [PubMed]
18. Brown, P.; Ackermann, D.; Finlayson, B. Calcium oxalate dihydrate (weddellite) precipitation. *J. Cryst. Growth* **1989**, *98*, 285–292. [CrossRef]
19. Šter, A.; Šafranko, S.; Bilić, K.; Marković, B.; Kralj, D. The effect of hydrodynamic and thermodynamic factors and the addition of citric acid on the precipitation of calcium oxalate dihydrate. *Urolithiasis* **2018**, *46*, 243–256. [CrossRef]
20. Stanković, A.; Kontrec, J.; Džakula, B.N.; Kovačević, D.; Marković, B.; Kralj, D. Preparation and characterization of calcium oxalate dihydrate seeds suitable for crystal growth kinetic analyses. *J. Cryst. Growth* **2018**, *500*, 91–97. [CrossRef]
21. Škrtić, D.; Marković, M.; Komunjer, L.; Füredi-Milhofer, H. Precipitation of calcium oxalates from high ionic strength solutions: I. Kinetics of spontaneous precipitation of calcium oxalate trihydrate. *J. Cryst. Growth* **1984**, *66*, 431–440. [CrossRef]
22. Škrtić, D.; Füredi-Milhofer, H.; Marković, M. Precipitation of calcium oxalates from high ionic strength solutions: V. The influence of precipitation conditions and some additives on the nucleating phase. *J. Cryst. Growth* **1987**, *80*, 113–120. [CrossRef]
23. Werner, H.; Bapat, S.; Schobesberger, M.; Segets, D.; Schwaminger, S.P. Calcium Oxalate Crystallization: Influence of pH, Energy Input, and Supersaturation Ratio on the Synthesis of Artificial Kidney Stones. *ACS Omega* **2021**, *6*, 26566–26574. [CrossRef] [PubMed] [PubMed Central]
24. Brečević, L.; Škrtić, D.; Garside, J. Transformation of calcium oxalate hydrates. *J. Cryst. Growth* **1986**, *74*, 399–408. [CrossRef]
25. Ibis, F.; Dhand, P.; Suleymanli, S.; van der Heijden, A.E.D.M.; Kramer, H.J.M.; Eral, H.B. A Combined Experimental and Modelling Study on Solubility of Calcium Oxalate Monohydrate at Physiologically Relevant pH and Temperatures. *Crystals* **2020**, *10*, 924. [CrossRef]

26. Brečević, L.; Kralj, D.; Garside, J. Factors influencing the distribution of hydrates in calcium oxalate precipitation. *J. Cryst. Growth* **1989**, *97*, 460–468. [CrossRef]
27. Walton, R.C.; Kavanagh, J.P.; Heywood, B.R.; Rao, P.N. Calcium oxalates grown in human urine under different batch conditions. *J. Cryst. Growth* **2005**, *284*, 517–529. [CrossRef]
28. Baumann, J.M.; Affolter, B.; Siegrist, H.-P. Measurement of metastability, growth and aggregation of calcium oxalate in native urine. A new approach for clinical and experimental stone research. *Urol. Int.* **1997**, *59*, 214–220. [CrossRef]
29. Robert, M.; Boularan, A.M.; Colette, C.; Averous, M.; Monnier, M. Urinary calcium oxalate saturation in 'stone formers' and normal subjects: An application of the Equil$_2$ program. *British J. Urol.* **1994**, *73*, 358–361. [CrossRef]
30. Christmas, K.G.; Gower, L.B.; Khan, S.R.; El-Shall, H. Aggregation and dispersion characteristics of calcium oxalate monohydrate: Effect of urinary species. *J. Colloid. Interface Sci.* **2002**, *256*, 168–174. [CrossRef]
31. Burns, J.R.; Finlayson, B. A proposal for a standard reference artificial urine in vitro urolithiasis experiments. *Investig. Urol.* **1980**, *18*, 167–169. [PubMed]
32. Isaacson, L.C. Urinary composition in calcific nephrolithiasis. *Investig. Urol.* **1969**, *6*, 356–363. [PubMed]
33. Doremus, R.H.; Teich, S.; Silvis, P.X. Crystallization of calcium oxalate from synthetic urine. *Investig. Urol.* **1978**, *15*, 469–472. [PubMed]
34. Miller, J.D.; Randolph, A.D.; Drach, G.W. Observations upon calcium oxalate crystallization kinetics in simulated urine. *J. Urol.* **1977**, *117*, 342–345. [CrossRef] [PubMed]
35. Barker, L.M.; Pallante, S.L.; Eisenberg, H.; Joule, J.A.; Becker, G.L.; Howard, J.E. Simple synthetic and natural urines have equivalent anticalcifying properties. *Investig. Urol.* **1974**, *12*, 79–81. [PubMed]
36. Rose, M.B. Renal stone formation. The inhibitory effect of urine on calcium oxalate precipitation. *Investig. Urol.* **1975**, *12*, 428–433. [PubMed]
37. Hassan, A.I.; Saleh, H.M. Production of Amino Acids and Nucleic Acids from Genetically Engineered Microbial Cells and their Relevance to Biodegradation. *Green Energy Environ. Technol.* **2023**, *2*, 1–47. [CrossRef]
38. Primiano, A.; Persichilli, S.; Ferraro, P.M.; Calvani, R.; Biancolillo, A.; Marini, F.; Picca, A.; Marzetti, E.; Urbani, A.; Gervasoni, J. A Specific Urinary Amino Acid Profile Characterizes People with Kidney Stones. *Dis. Markers.* **2020**, *2020*, 8848225. [CrossRef] [PubMed] [PubMed Central]
39. Fleming, D.E.; van Bronswijk, W.; Ryall, R.L. A comparative study of the adsorption of amino acids on to calcium minerals found in renal calculi. *Clinical Sci.* **2001**, *101*, 159–168. [CrossRef]
40. Guo, S.; Ward, M.D.; Wesson, J.A. Direct visualization of calcium oxalate monohydrate crystallization and dissolution with atomic force microscopy and the role of polymeric additives. *Langmuir* **2002**, *18*, 4284–4291. [CrossRef]
41. Marković, M.; Komunjer, L.; Füredi-Milhofer, H.; Škrtić, D.; Sarig, S. Precipitation of calcium oxalate from high ionic strength solutions VII. The influence of glutamic acid. *J. Cryst. Growth* **1988**, *88*, 118–124. [CrossRef]
42. Taranets, X.Y.; Dryhailo, M.K.; Bezkrovna, O.M.; Pritula, I.M. The role of amino acids in the processes of nucleation of pathogenic crystals of calcium oxalate monohydrate under human body imitating conditions. *J. Cryst. Growth* **2023**, *602*, 126973. [CrossRef]
43. Grases, F.; March, J.G.; Bibiloni, F.; Amat, E. The crystallization of calcium oxalate in the presence of aminoacids. *J. Cryst. Growth* **1988**, *87*, 299–304. [CrossRef]
44. Laube, N.; Mohr, B.; Hesse, A. Laser-probe-based investigation of the evolution of particle size distributions of calcium oxalate particles formed in artificial urines. *J. Cryst. Growth* **2001**, *233*, 367–374. [CrossRef]
45. Golovanova, O.A.; Punin, Y.U.O.; Vystoskiy, A.S.; Khannanov, V.R. Effect of Organic and Inorganic Impurities on the Nucleation of Calcium Oxalate Monohydrate. *Chem. Sustain. Dev.* **2011**, *19*, 463–470.
46. Golovanova, O.A.; Achkasova, E.Y.; Punin, Y.O.; Zhelyaev, E.V. Main regularities of crystallization of calcium oxalate in the presence of amino acids. *Crystallogr. Rep.* **2006**, *51*, 348–354. [CrossRef]
47. Shee, K.; Stoller, M.L. Perspectives in primary hyperoxaluria—Historical, current and future clinical interventions. *Nat. Rev. Urol.* **2022**, *19*, 137–146. [CrossRef] [PubMed]
48. Stanković, A.; Šafranko, S.; Kontrec, J.; Njegić Džakula, B.; Lyons, D.M.; Marković, B.; Kralj, D. Calcium oxalate precipitation in model systems mimicking the conditions of hyperoxaluria. *Cryst. Res. Technol.* **2019**, *54*, 1800210. [CrossRef]
49. Pierratos, A.E.; Khalaff, H.; Cheng, P.T.; Psihramis, K.; Jewett, M.A. Clinical and biochemical differences in patients with pure calcium oxalate monohydrate and calcium oxalate dihydrate kidney stones. *J. Urol.* **1994**, *151*, 571–574. [CrossRef] [PubMed]
50. Matijaković Mlinarić, N.; Šafranko, S.; Vidas, B.; Goman, D.; Jokić, S.; Kontrec, J.; Stanković, A. Precipitation of Calcium Oxalate Monohydrate Under Nearly the Same Initial Supersaturation. *Croat. Chem. Acta* **2021**, *94*, 59–66. [CrossRef]
51. Macrae, C.F.; Bruno, I.J.; Chisholm, J.A.; Edgington, P.R.; McCabe, P.; Pidcock, E.; Rodriguez-Monge, L.; Taylor, R.; van de Streek, J.; Wood, P.A. Mercury CSD 2.0– new features for the visualization and investigation of crystal structures. *J. Appl. Cryst.* **2008**, *41*, 466–470. [CrossRef]
52. Echigo, T.; Kimata, M.; Kyono, A.; Shimizu, M.; Hatta, T. Re-investigation of the crystal structure of whewellite [$Ca(C_2O_4)\cdot H_2O$] and the dehydration mechanism of caoxite [$Ca(C_2O_4)\cdot 3H_2O$]. *Mineral. Mag.* **2005**, *69*, 77–88. [CrossRef]
53. Shen, Y.; Li, S.; Xie, A.; Xu, W.; Qiu, L.; Yao, H.; Yu, X.; Chen, Z. Controlled growth of calcium oxalate crystal in bicontinuous microemulsions containing amino acids. *Colloids Surf. B Biointerfaces* **2007**, *58*, 298–304. [CrossRef] [PubMed]
54. Shen, Y.; Yue, W.; Xie, A.; Li, S.; Qian, Z. Effects of amino acids on crystal growth of CaC_2O_4 in reverse microemulsion. *Colloids Surf. B. Biointerfaces* **2005**, *45*, 120–124. [CrossRef]

55. Ouyang, J.M.; Duan, L.; Tieke, B. Effects of carboxylic acids on the crystal growth of calcium oxalate nanoparticles in lecithin−water liposome systems. *Langmuir* **2003**, *19*, 8980–8985. [CrossRef]
56. Monné, M.; Vozza, A.; Lasorsa, F.M.; Porcelli, V.; Palmieri, F. Mitochondrial Carriers for Aspartate, Glutamate and Other Amino Acids: A Review. *Int. J. Mol. Sci.* **2019**, *20*, 4456. [CrossRef]
57. Sun, X.-Y.; Zhang, C.-Y.; Bhadja, P.; Ouyang, J.-M. Preparation, properties, formation mechanisms, and cytotoxicity of calcium oxalate monohydrate with various morphologies CrystEngComm 2018, 20, 75–87. *CrystEngComm* **2018**, *20*, 75–87. [CrossRef]
58. Tazzoli, V.; Domenegheti, C. The crystal structures of whewellite and weddellite: Re-examination and comparison. *Am. Mineral.* **1980**, *65*, 327–334.
59. Deganello, S.; Piro, O.E. The crystal structure of calcium oxalate monohydrate (whewellite). *N. Jb. Miner. Mh. H.* **1981**, *2*, 81–88.
60. Fischer, V.; Landfester, K.; Muñoz-Espí, R. Stabilization of calcium oxalate metastable phases by oligo (L-glutamic acid): Effect of peptide chain length. *Cryst. Growth Des.* **2011**, *11*, 1880–1890. [CrossRef]
61. Sargut, S.T.; Sayan, P.; Kiran, B. Influence of essential and non-essential amino acids on calcium oxalate crystallization. *Cryst. Res. Technol.* **2010**, *45*, 31–38. [CrossRef]
62. Sayan, P.; Titiz Sargut, S.; Kiran, B. Calcium oxalate crystallization in the presence of amino acids, proteins and carboxylic acids. *Cryst. Res. Technol.* **2009**, *44*, 807–817. [CrossRef]
63. Golovanova, O.A.; Punin, Y.O.; Izatulina, A.R.; Korol'kov, V.V. Crystallization of calcium oxalate monohydrate in the presence of amino acids: Features and regularities. *J. Struct. Chem.* **2014**, *55*, 1356–1370. [CrossRef]
64. Wei, X.; Yang, J.; Li, Z.; Su, Y.; Wang, D. Comparison investigation of the effects of ionic surfactants on the crystallization behavior of calcium oxalate: From cationic to anionic surfactant. *Colloids Surf. A Physicochem. Eng. Asp.* **2014**, *401*, 107–115. [CrossRef]
65. Sun, X.Y.; Xu, M.; Ouyang, J.M. Effect of Crystal Shape and Aggregation of Calcium Oxalate Monohydrate on Cellular Toxicity in Renal Epithelial Cells. *ACS Omega* **2017**, *30*, 6039–6052. [CrossRef] [PubMed] [PubMed Central]
66. Sheng, X.; Jung, T.; Wesson, J.A.; Ward, M.D. Adhesion at calcium oxalate crystal surfaces and the effect of urinary constituents. *Proc. Natl. Acad. Sci. USA* **2005**, *11*, 267–272. [CrossRef] [PubMed] [PubMed Central]
67. Qiu, S.R.; Wierzbicki, A.; Salter, E.A.; Zepeda, S.; Orme, C.A.; Hoyer, J.R.; Nancollas, G.H.; Cody, A.M.; De Yoreo, J.J. Modulation of calcium oxalate monohydrate crystallization by citrate through selective binding to atomic steps. *J. Am. Chem. Soc.* **2005**, *127*, 9036–9044. [CrossRef]
68. Jung, T.; Sheng, X.; Choi, C.K.; Kim, W.S.; Wesson, J.A.; Ward, M.D. Probing crystallization of calcium oxalate monohydrate and the role of macromolecule additives with in situ atomic force microscopy. *Langmuir* **2004**, *20*, 8587–8596. [CrossRef]